A molecular dynamics simulation interpretation of neutron and x-ray diffraction measurements on single phase Y_2O_3–Al_2O_3 glasses

2009 J. Phys.: Condens. Matter 21 205102

(http://iopscience.iop.org/0953-8984/21/20/205102)

J. Phys.: Condens. Matter **21** (2009) 205102 (9pp) doi:10.1088/0953-8984/21/20/205102

A molecular dynamics simulation interpretation of neutron and x-ray diffraction measurements on single phase Y_2O_3–Al_2O_3 glasses

Jincheng Du[1], Chris J Benmore[2], Rene Corrales[3], Robert T Hart[2,4] and J K Richard Weber[2,5]

[1] Department of Materials Science and Engineering, University of North Texas, Denton, TX 76203, USA
[2] Advanced Photon Source, Argonne National Laboratory, 9700 South Cass Avenue, Argonne, IL 60439, USA
[3] Department of Chemistry, University of Arizona, Tucson, AZ 85721, USA
[4] The Shepherd Chemical Company, 4900 Beech Street, Norwood, OH 45212, USA
[5] Materials Development Incorporated, Arlington, Heights, IL 60004, USA

E-mail: Jincheng.du@unt.edu and benmore@aps.anl.gov

Received 5 February 2009, in final form 10 March 2009
Published 8 April 2009
Online at stacks.iop.org/JPhysCM/21/205102

Abstract

Molecular dynamics simulations and complementary neutron and x-ray diffraction studies have been carried out within the single phase glass forming range of $(Y_2O_3)_x(Al_2O_3)_{(100-x)}$, for $x = 27$ and 30. For $x = 27$, the experimental Al–O and Y–O coordination numbers are found to be 4.9 ± 0.2 and 6.9 ± 0.4 respectively, compared to 4.4 and 6.8 obtained from the simulation. Similar results were found for $x = 30$. An R-factor analysis showed that the simulation models agreed to within ~6% of the diffraction data in both cases. The Al–O polyhedra are dominated by fourfold and fivefold species and the Y–O local coordinations are dominated by sixfold, sevenfold and eightfold polyhedra. Analysis of the oxygen environments reveals a large number of combinations, which explains the high entropy of single phase yttrium aluminate glasses and melts. Of these, the largest variation between $x = 27$ and 30 is found in the number of aluminum oxygen triclusters (oxygens bonded to three Al) and oxygens surrounded by three Y and a single Al. The most abundant connections are between the AlO_x and YO_y polyhedra of which 30% are edge shared. The majority of AlO_x–AlO_x connections were found to be corner shared.

(Some figures in this article are in colour only in the electronic version)

1. Introduction

The atomic structure of yttria–alumina $(Y_2O_3)_x(Al_2O_3)_{(100-x)}$ glasses and melts have been the subject of intense scrutiny following the observations of a potential first order liquid–liquid phase transition at low Y_2O_3 contents [1, 2]. Aasland and McMillan [1] formed glasses in a hot stage microscope and found that over the composition range $24 < x < 32$ they became phase separated. Samples outside this range crystallized upon quenching the melt. The minority phase accounts for up to ~15% by volume and appears approximately circular under electron and optical microscopy with dimensions from ~1 to ~50 μm, consistent with binodal (nucleation and growth) phase separation into spherical droplets within a continuous matrix. The composition of the first and second glassy forms have been shown to be essentially identical [1, 3]. By altering the quench rate, single phase glasses have also been formed around $x \sim 30$.

Neutron scattering studies on a two phase $x = 20$ glass (containing some small crystallites) and a single phase $x = 25$

glass concluded there was no difference in the average Al–O coordination number between the two materials [4]. NMR has shown that a substantial fraction of the aluminum environments are consistent with mainly 4-coordinate (∼68%) and 5-coordinate (25%) aluminum, with the rest being 6-coordinate [5]. This is in approximate agreement with previously published neutron and x-ray diffraction data which gives values between 4.0 [6] and 4.4 [4]. Johnson and Kriven have studied the crystallization kinetics of $Y_3Al_5O_{12}$ ($x = 37.5$) and reported the formation of nanocrystals and also 'amorphous regions of different contrast yet with the same composition' [7] in agreement with the polyamorphic behavior found by Aasland and McMillan [1]. Weber *et al* [6] performed neutron and x-ray diffraction studies on single phase $x = 27$ and two phase $x = 37.5$ (∼1% crystallinity and ∼15% of the second phase) glasses produced by levitation melting, indicating changes in the Y–O coordination and connectivity. Polarizable ion model molecular dynamics simulations [8, 21] on $x = 20, 25$ glasses generally support these findings, showing significant changes in the Y–Al and Y–Al correlations, a subtle change in the Y–O coordination and no change in the Al–O coordination number.

Nagashio and Kuribayashi [9] also produced single phase glasses using containerless techniques within the compositional range $0.25 < x < 0.325$ and found the glasses in the range $0.325 < x < 0.375$ contained small $Y_3Al_5O_{12}$ crystalline inclusions. Skinner *et al* [10] have confirmed these latter observations by producing homogeneous and transparent single phase glasses over the optimum glass forming range between $0.27 < x < 0.33$ and cloudy mixtures of up to 40 μm crystalline $Y_3Al_5O_{12}$ droplets embedded in a glass matrix between $0.33 < x < 0.375$. At lower Y_2O_3 concentrations of $x = 0.24$ cloudy two phase glasses were found. Most recently, Greaves *et al* [2] detected evidence of a first order liquid–liquid phase transition *in situ* at the composition $x = 0.20$.

The aim of the current paper is to characterize the structure of the single phase glasses in detail and identify the structural features subject to the largest variability in this narrow range. Therefore, we have undertaken high-energy x-ray and neutron diffraction experiments alongside molecular dynamics simulations on glasses of composition $x = 27$ and 30 in order to discern the inter-polyhedral ordering that describes the connectivity of the glass.

2. Methods

2.1. Synthesis

The two yttria alumina (YA) compositions studied as given in table 1 were prepared in 5 g batches by mixing 99.99% pure Y_2O_3 and Al_2O_3 powders (Cerac, Inc., Milwaukee, WI). Weighed powders were homogenized in a ball mill and fused in a laser hearth into a crystalline boule. The resulting boule was ground to a powder, remelted in the hearth in the same manner and then crushed into pieces 2–3.5 mm in diameter. The 2–3.5 mm diameter samples were levitated in O_2 gas in a conical nozzle levitator and were heated and melted with a partially focused continuous wave CO_2 laser. The liquid was superheated by ∼50 K to ensure complete melting, held for ∼10 s, and then cooled by blocking the heating laser to achieve cooling rates of about 100 K s^{-1} for all samples. Sample temperatures were recorded at 30 Hz with an automatic optical pyrometer (of effective wavelength ∼650 nm).

Table 1. Compositions and densities of samples studied.

Sample	Y_2O_3 (mol%)	Al_2O_3 (mol%)	Density (g cm^{-3})	Number density (atom Å^{-3})
YA30	30.4 ± 0.3	69.6 ± 0.4	3.937 ± 0.013	0.0849 ± 0.0003
YA27	26.5 ± 0.2	73.5 ± 0.2	3.807 ± 0.001	$0.085\,04 \pm 0.000\,02$

Chemical compositions of the resulting glass samples were analyzed using a Cameca SX-50 electron microprobe. Quantitative, wavelength-dispersive analyses were performed at 20 keV with a beam current of 10 nA having a diameter of ∼1 μm. Measurements were obtained on three glass spheroids for each composition, at several points across the diameter of the polished and carbon coated surfaces. Single crystal YAG was used as the standard for Al_2O_3 and Y_2O_3 in conjunction with conventional ZAF matrix corrections. The densities were determined with a pycnometer using distilled water as the immersion fluid, see table 1. Here we use the representation YA27 to refer to $(Y_2O_3)_{27}(Al_2O_3)_{73}$. Both the YA27 and YA30 samples were verified to be homogeneous single phase glasses by optical microscopy.

Table 1 presents compositions of the glasses as determined by EDS together with the measured densities. It can be seen that the compositions are close to the nominal batch targets.

2.2. Diffraction experiments

High-energy x-ray diffraction data were collected at the 11-ID-C beamline of the Advanced Photon Source using a 1.0 mm × 0.5 mm beam of 117 keV photons [24]. The glass samples were contained in thin-walled (10 μm) glass tubes (Muller Glas Technik, Dotternhausen, Germany). An independent background measurement was made and the background subtracted data were corrected for polarization and geometric and relativistic effects. Normalization was accomplished by scaling the high-Q scattering to tabulated Compton scattering values. The pseudonuclear total scattering factors were created using the atomic form factors of Hubbell [19]. These manipulations are implemented within the Isomer-X software [25].

Neutron diffraction data were collected on the glass, liquids and amorphous diffractometer (GLAD) at the Intense Pulsed Neutron Source using a 10 mm × 13 mm beam [26]. About 1 g of each sample was placed in thin-walled (0.005″) vanadium sample containers and aligned with the incident beam. The data were corrected for container scattering, absorption, multiple scattering, inelastic effects and normalized to the incoherent scattering from a vanadium rod using software developed for analysis of data from this instrument [27].

2.3. Molecular dynamics simulations

Classical molecular dynamics (MD) simulations were carried out to simulate the glasses using potentials based on

Table 2. Potential parameters used in the MD simulations.

Pairs	A (eV)	ρ (Å)	C (eV Å^6)
$Al^{2.4}$–$O^{-1.2}$	13 702.905	0.193 817	54.681
$O^{-1.2}$–$O^{-1.2}$	2 029.2204	0.343 645	192.58
$Y^{1.8}$–$O^{-1.2}$	29 526.977	0.211 377	50.477

point charge Born model. The interatomic potential is a combination of long-range Coulombic interaction and a short-range Buckingham potential with full potential having the form of

$$V(r) = \frac{Z_i Z_j e^2}{4\pi\varepsilon_0 r} + A\exp(-r/\rho) - C/r^6 \qquad (1)$$

where r is the distance between atom i and j, Z_i, Z_j are the effective charges, A, ρ and C are Buckingham parameters (see table 2). The atomic charges and potential parameters were derived from combining efforts of *ab initio* calculations and empirically fitting structural and physical properties of the minerals Al_2O_3 and Y_2O_3 and are listed in table 1. Partial covalency of the bondings in the oxide system is modeled by reduced atomic charges. Similar partial charge pair potentials have been successfully used to study the structure and dynamics of silicate glasses [11–14]. The potentials were first tested for their abilities to reproduce the related crystalline structures and properties including bulk moduli of the related yttrium aluminum garnet ($Y_3Al_5O_{12}$) [15], yttrium aluminum perovskite ($YAlO_3$, YAP) and monoclinic $Y_4Al_2O_9$ phases. To properly model the glass melt at high temperature, the original Buckingham short-range interaction was modified to overcome the characteristic fusion of atoms at low r when the power term overrides the exponential term. This was achieved by splicing a function of the form $Br^n + Dr^2$ at low r by properly choosing the splice point at the deflection point of the force between the first maximum and the first minimum [14] of the original Buckingham potential. The B, n and D parameters are chosen to make the potential, force and force constant at the splice point continuous.

Each simulation cell contains 2500 atoms. The resulting cubic cells had the volume of around 30 Å^3 based on the experimental composition and density listed in table 1. The initial configuration of each glass was randomly generated with constraints between atom pairs to avoid overlapping atoms. The dynamic simulations were executed in 2 fs time steps. Each configuration was first equilibrated at 6000 K for 80 000 steps and then melted at 4000 K for 120 000 steps. The melt was quenched to 300 K within 185 000 steps, with a nominal cooling rate 10 K ps^{-1}. The glasses were equilibrated for another 80 000 steps at 300 K. The canonical (constant number volume and temperature (NVT)) ensemble was used for equilibration and cooling process with a Nose–Hoover thermostat [16, 17], while the microcanonical (constant number, volume and energy (NVE)) ensemble was used in the production runs of the melt and the final glasses. The structure and dynamics during the glass formation processes were monitored. While only the analyses over the last 400 configurations (every 50th of the final 20 000 steps at 300 K) are presented as the final glass structure. Structural analysis

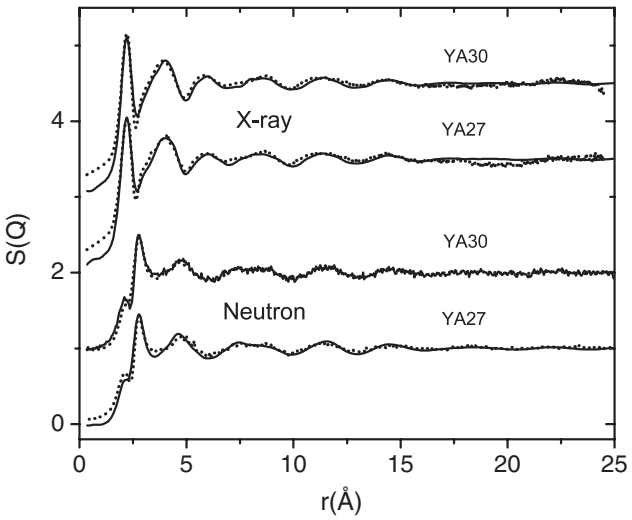

Figure 1. Total structure factors for $(Y_2O_3)_x(Al_2O_3)_{(100-x)}$ glasses. The experimental data are shown as solid lines and the simulations are dashed lines. The simulation total structure factors were generated using the Faber–Ziman formalism after inverse Fourier transformation of the partial structure factors at $r_{max} = 15$ Å (see text).

such as pair distribution functions $g(r)$, coordination number, and bond angle distributions were obtained by averaging over the 400 configurations for each of the simulated glasses.

Partial structure factors were calculated by Fourier transformation of the pair distribution functions

$$S_{ij}(Q) = 1 + \rho_o \int_0^R 4\pi r^2 [g_{ij}(r) - 1] \frac{\sin(Qr)}{Qr} \frac{\sin(\pi r/R)}{\pi r/R} \mathrm{d}r \qquad (2)$$

in which $g_{ij}(r)$ is the pair distribution function of atom pair i and j, Q is the scattering vector, ρ_o is the average atom number density, R is the maximum value of the integration in real space which is set to half of the size of one side of the simulation cell. The $\frac{\sin(\pi r/R)}{\pi r/R}$ part is a Lorch type window function [29] to reduce the effect due to finite cutoff of r. The total neutron structure factor is calculated by,

$$S_N(Q) = \left(\sum_{i=1}^{n} c_i b_i\right)^{-2} \sum_{i,j=1}^{n} c_i c_j b_i b_j S_{ij}(Q) \qquad (3)$$

in which c_i and c_j are the fraction of atoms, b_i and b_j are neutron scattering lengths, for element i and j, respectively. The neutron scattering lengths used are 5.803, 3.449, and 7.75 fm for oxygen, aluminum and yttrium, respectively [18]. For x-rays the b_i values were replaced with the atomic form factors $f_i(Q)$ [19].

3. Results

3.1. Reciprocal space

Figure 1 shows the measured diffraction data compared to the simulation data in Q-space. It can be seen that the general agreement between the experiments and the simulations is good, although there is a small mismatch in the low-Q x-ray and simulation comparison which may arise from the choice of form factor or limited simulation box size.

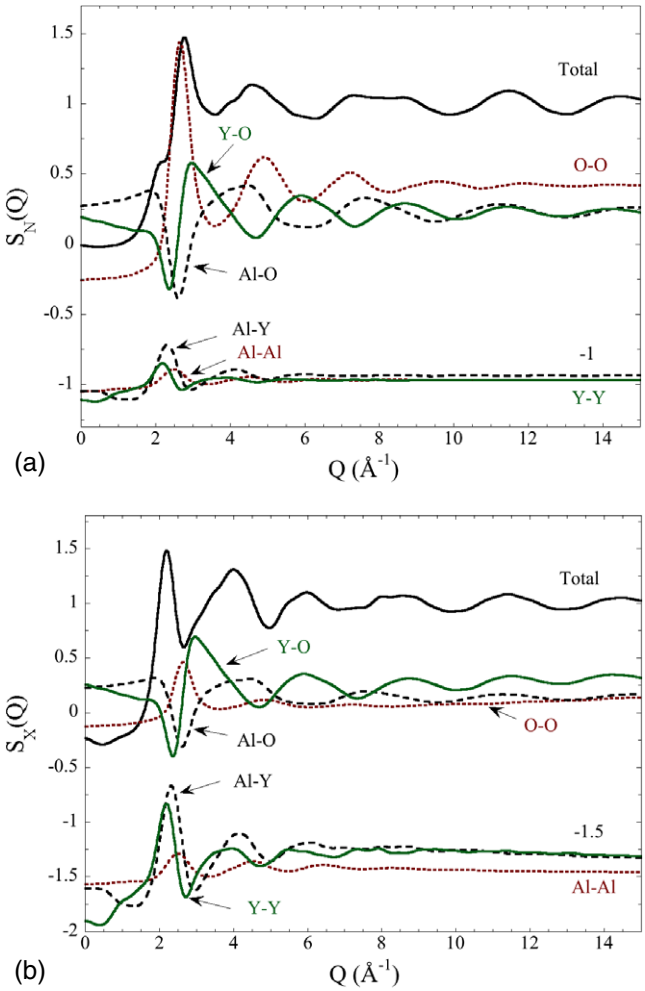

Figure 2. Total and weighted partial neutron (a) and x-ray (b) structure factors for YA30 glass.

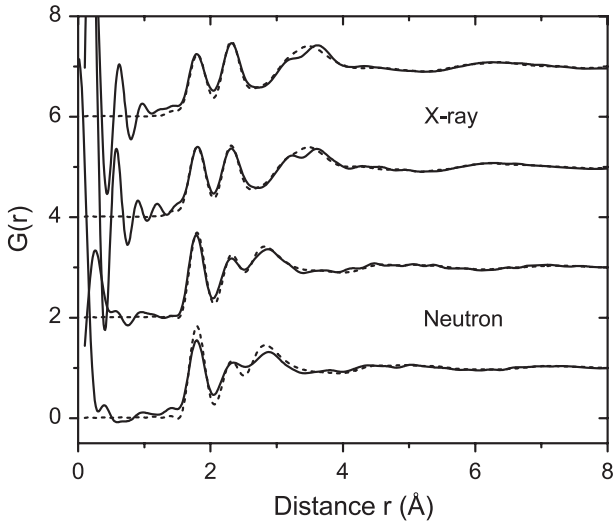

Figure 3. Radial distribution functions for $(Y_2O_3)_x(Al_2O_3)_{(100-x)}$ glasses. These transforms have been made from the data shown in figure 1. The experimental data are shown as solid lines and the simulations are shown as dashed lines.

The partial structure factor contributions obtained from the molecular dynamics simulations, compared to the total neutron and x-ray structure factors for the YA30 glass are shown in figure 2. Similar results were found for YA27. The first feature in the neutron total structure factor is the principal peak at 2.8 Å^{-1} with a low-Q shoulder located at 2.2 Å^{-1}. The first peak is dominated by the O–O partial structure factor with other positive contributions from the three cation–cation partial structure factors, and the Y–O and Y–Al partial structure factors contributing as dips in the low-Q region. The similarity of the neutron scattering length of the O (5.805 fm), Al (3.449 fm) and Y (7.75 fm) means the Faber–Ziman [28] factors of each atom pair are heavily influenced by the mole fraction of each type of element. For the YA30 glass, the Faber–Ziman factors are 0.418, 0.230, 0.226 for the O–O, Al–O and Y–O pairs, respectively, and 0.032, 0.062 and 0.306 for the Al–Al, Al–Y and Y–Y pairs, respectively. The features in the higher Q region (>7 Å^{-1}) are dominated equally by the Al–O and Y–O contributions. In the x-ray case the first (principal) peak is at 2.2 Å^{-1} and the main contributions arise from the Y–Y and Y–Al partial structure factors. The dominance of the contributions of the yttrium inclusion pairs is simply due to the much larger atomic number of yttrium (39) than that of Al (13) and O (8). In addition, the major peak in neutron structure factor at 2.2 Å^{-1} (dominated by the O–O) is missing in the x-ray case largely due to a cancelation by the Al–O partial structure factor. The oscillations at high Q (>7 Å^{-1}) in the x-ray case is dominated by the Y–O partial structure factor with a smaller contribution coming from Al–O.

3.2. Pair distribution functions

In figure 3, the Fourier transformations of the neutron and x-ray data are shown compared to simulation data treated in an identical manner with a Lorch function applied at high-Q to minimize truncation effects [29]. It can be seen that very slightly narrower Al–O and Y–O correlations appear in the simulations, and the experimental data show more clearly resolved metal–metal correlations. The experimental O–O correlations peak are about 2.9 Å whereas in the simulations this peak is at a slightly shorter distance of 2.8 Å. Due to the different atomic scattering factors from x-rays and neutrons, the contributions of different atom pairs to the total structure factors or total correlation function is different as shown in the Faber–Ziman factors. By combining the structural information from this two different types of diffraction experiment, it is sometimes possible to remove contributions of certain atom pairs and thus able to obtain desirable structure information [30]. This has been performed for the current glass systems by removing the O–O contribution since there is considerable overlap the O–O first peak (at around 2.8 Å) and the Y–O first peak (at 2.3 Å). Fourier transformation of the O–O removed structure factor lead to the pair distribution function shown in figure 4. The first and second peak, corresponding to the contribution of the first peaks of Al–O and Y–O partial distribution function, agree well between experimental and simulations.

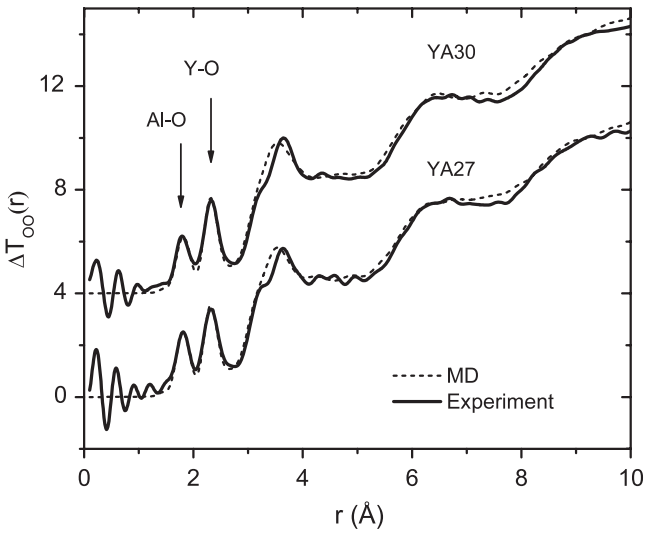

Figure 4. First order difference functions with the O–O removed for $(Y_2O_3)_x(Al_2O_3)_{(100-x)}$ glasses. These curves have been generated from the $\Delta S_{OO}(Q)$ functions as described in the text via first order differences of the x-ray and neutron total structure factors. The experimental data are shown as solid lines and the simulations are shown as dashed lines.

Wright has suggested calculating an R-factor which is an indication of the accuracy of computer generated models compared to measured neutron and x-ray pair distribution functions ([31], equation (2)), which should be quoted when claiming good agreement. We have applied this formula to the measured first order difference function shown in figure 4 and find that the agreement between the MD model and the combined neutron/x-ray function is 6.2% (YA30) and 6.5% (YA27). The MD partial pair distribution function contributions to the total neutron and x-ray functions are shown in figure 5.

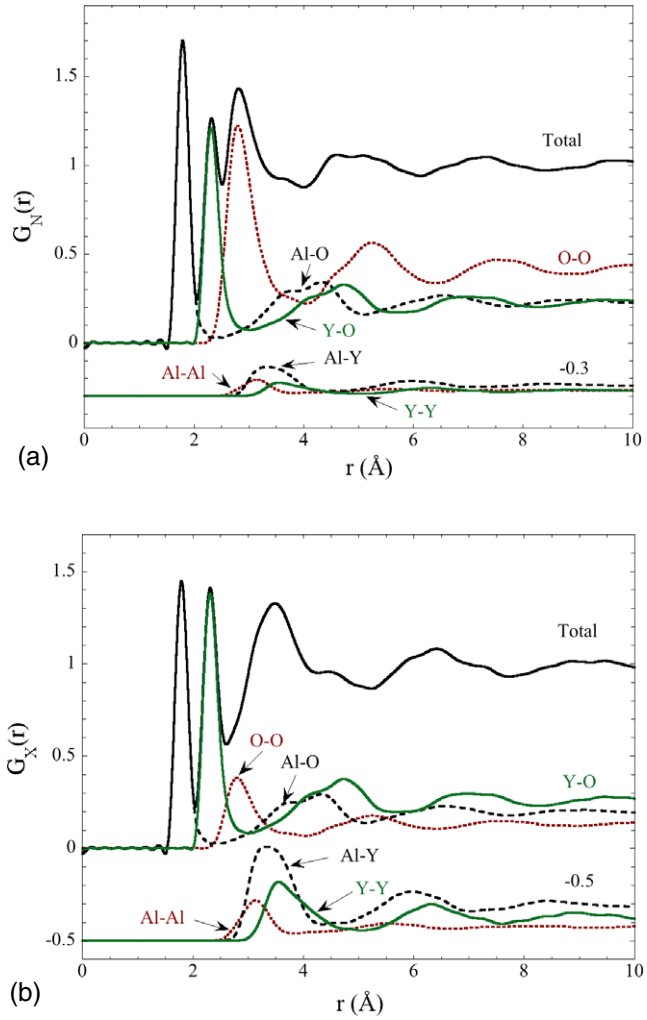

Figure 5. Neutron (a) and x-ray (b) broadened total and pair distribution functions for YA30 glass.

3.3. Bond lengths and coordination numbers

The coordination numbers were determined from the integrated peak areas for the Al–O and Y–O peaks from both the neutron and x-ray data in real space. Gaussian functions were found to be reasonable representations of the peaks for the neutron data. For the simulated x-ray data, Gaussian functions at the Al–O and Y–O bond lengths were Fourier transformed into Q space and convoluted with the Q-dependent form factors for isotropic x-ray scattering from the compositions studied, then inverse Fourier transformed back to r-space. The integrated areas of these peak shapes were converted to coordination numbers by assuming x-ray scattering lengths in the $Q = 0$ approximation. The fit region was from 1 to 3 Å and included a third peak for each data set centered at about 2.9 Å to account for overlap between the Y–O and O–O correlations. The fits were made in a simultaneous manner by adjusting the candidate coordination number for each ion until the total residual was minimized.

The diffraction data yield an Al–O distance of 1.80 Å for YA27 and 1.79 Å for YA30, which compares well with the value of 1.80 Å for both compositions from the MD simulation. The experimental aluminum–oxygen coordination numbers are found to be $n_{AlO} = 4.9 \pm 0.2$ for YA27 and 4.8 ± 0.2 for YA30, which are slightly larger than the values from simulation which gives 4.42 (YA27) and 4.48 (YA30). The Y–O bond length and coordination number were obtained by combining x-ray and neutron diffraction data and removing the O–O correlations [30]. The Y–O bond length was found to be 2.32 Å for both compositions in exact agreement with the simulation results. The experimental yttrium–oxygen coordination numbers are found to be $n_{YO} = 6.8 \pm 0.4$ for YA27 and 7.0 ± 0.4 for YA30, which is also in good agreement with the simulation results of 6.83 (YA27) and 6.89 (YA30). The Al–O and Y–O bond lengths and coordination numbers agree well with those determined experimentally using neutron and x-ray diffraction methods in this work (table 3) and those from literature [4, 6].

Cristiglio *et al* [20] have performed *ab initio* MD simulations based on density functional theory for Y_2O_3–Al_2O_3 melts with compositions of $x = 15$, 20 and 25. The results are in reasonable agreement with high temperature neutron diffraction data performed using an aerodynamic levitator in the same study. These authors find cation

Table 3. Cation environments around oxygen.

	Coordination number			Oxygen environments (%)						
Glass	Al	Y	Total	1Al2Y	2Al1Y	3Al	1Al3Y	2Al2Y	3Al1Y	Others
YA30	2.08	1.39	3.47	8.2	29.0	14.6	11.1	20.4	11.5	5.2
YA27	2.16	1.21	3.37	7.1	32.3	20.1	7.0	18.1	9.4	6.0

coordination numbers of $n_{\mathrm{AlO}} = 4.2 \pm 0.3$ at 1.81 Å and $n_{\mathrm{YO}} = 6.4 \pm 1.0$ at 2.34 Å which are in good agreement with the findings of this work [20]. The partial pair distribution functions presented here are qualitatively very similar to those reported by Wilson and McMillan, obtained using a polarizable ion model (PIM) performed on compositions at $x = 20$ and 25 [21]. The PIM structure models give a slightly higher cation–oxygen coordination numbers of $n_{\mathrm{AlO}} = 5.4$ at 1.81 Å and $n_{\mathrm{YO}} = 8.0$ at 2.32 Å than found in this study. However our simulation results show significantly better agreement with the measured diffraction data than either of these two previous molecular dynamics simulations on the Y_2O_3–Al_2O_3 system.

4. Discussion

4.1. Polyhedral distributions

Results of oxygen coordination number distributions around aluminum ions were obtained by analyzing the final configurations of the simulated glasses at 300 K. There exist 4-, 5- and 6-coordinated aluminum ions, with percentages of 63.1%, 31.2% and 5.7% respectively, for the YA27 composition, determined with an Al–O cut off at 2.4 Å. Similar values of 58.2%, 36.5% and 5.3%, were obtained for the YA30 composition. Several ^{27}Al NMR studies have confirmed the existence of 4-, 5- and 6-coordinated aluminum sites in yttrium aluminate glasses [5, 22]. By fitting the NMR spectra, it was found that the aluminum coordination numbers were around 4.4 and changed little with composition, agreeing well with our simulation results [5]. We note that a maximum of the 5-coordinated aluminum was observed for the YA29 composition experimentally [5]. Although the average coordination numbers from NMR and our MD simulation agree well, the percentage of 4-coordinated aluminum is higher and 5-coordinated aluminum is lower in the simulation than from the NMR study [5]. For example, the 4-, 5-, and 6-coordinated aluminum for the YA28.5 composition were found to be in the ratio 68 ± 2%, 27 ± 3%, and 6 ± 2%, respectively [5]. In related crystalline systems, aluminum ions are 6-coordinated in α-Al_2O_3 and YAP ($YAlO_3$) and 4- (60%) and 6-coordinated (40%) in YAG ($Y_3Al_5O_{12}$). Hence the aluminum coordination number is reduced during melting and remains so in the subsequently formed glass.

The distribution of the yttrium–oxygen coordination number for the YA27 simulated glass is dominated by 6-, 7- and 8-fold coordinate species in proportions of 30.6%, 49.7%, and 17.8%, respectively, calculated with a cut off at 3.0 Å. Similar values of 29.4%, 49.8% and 17.0%, were obtained for the YA30 composition. The average yttrium coordination number from MD simulation of 6.8 is consistent with previous diffraction studies, which have values ranging from 6 to 7 [4, 6]. The Y–O bond length from the simulation is 2.32 Å, slightly longer than those found in diffraction studies (2.28 Å) [4, 6]. In crystalline phases, yttrium ions are 8-coordinated in Y_2O_3, YAP and YAG and 6- and 7-coordinated in monoclinic $Y_4Al_2O_9$. The Y–O bond length in these crystalline phases ranges from 2.17 to 2.41 Å, with the Y–O bond length in the glasses falling into this range.

4.2. Oxygen environments

From the simulated glass structure it is possible to perform detailed analyses of the oxygen environments, which is shown in table 3. The average cation coordination number decreases slightly from 3.47 for YA30 to 3.37 for YA27. The cation coordination number around oxygen ranges from 2 to 5 but majority (over 95%) of these are 3 and 4. The main oxygen environment combinations are $OAlY_2$, OAl_2Y, OAl_3, $OAlY_3$, OAl_2Y_2 and OAl_3Y.

From YA27 to YA30, the percentages of OAl_3 and $OAlY_3$ change more than the other oxygen environments. The percentage of OAl_3 (three aluminum ions bonded to one oxygen ion—an oxygen tricluster) doubled from 10.3% to 20.1% and the percentage of $OAlY_3$ decreased by almost half from 13.2% to 7.0%. Examples of an aluminum–oxygen network and an aluminum oxygen tricluster are shown in figure 7(a). The aluminum oxygen tricluster (OAl_3) has been previously been observed in alumina-silicate glasses [23]. It is characteristic of the aluminum oxygen network. The increase of concentration of aluminum oxygen triclusters indicates a stronger aluminum oxygen network due to its low coordination number. There is also a small fraction of oxygen ions (around 1%) that are two coordinated by cations. It is found that most (over 99%) of these oxygen ions are coordinated by two aluminum cations. For comparison, in crystalline phases, the oxygen environments are limited to a few of combinations: one (OY_2Al_2) in YAG crystal, one (OAl_3) in α-Al_2O_3 and two (OY_2Al_2 and OY_3Al_2) in YAP crystal. The limited number of distinct oxygen environments in these crystals is in contrast with the larger number of oxygen environments and varied distributions in the simulated glasses.

4.3. Bond angle distributions and polyhedral connectivity

Figure 6 shows the bond angle distributions (BADs) of the simulated glasses. The O–Al/Y–O bond angle distributions describe the cation–oxygen polyhedra, while the Al/Y–O–Al/Y bond angle distributions show how the neighboring cation polyhedra are connected. The O–Al–O BAD has a major peak at around 100° that represents the [AlO_4] tetrahedral coordination and a minor peak at around 165° with contributions from 5-coordinated aluminum. Two peaks

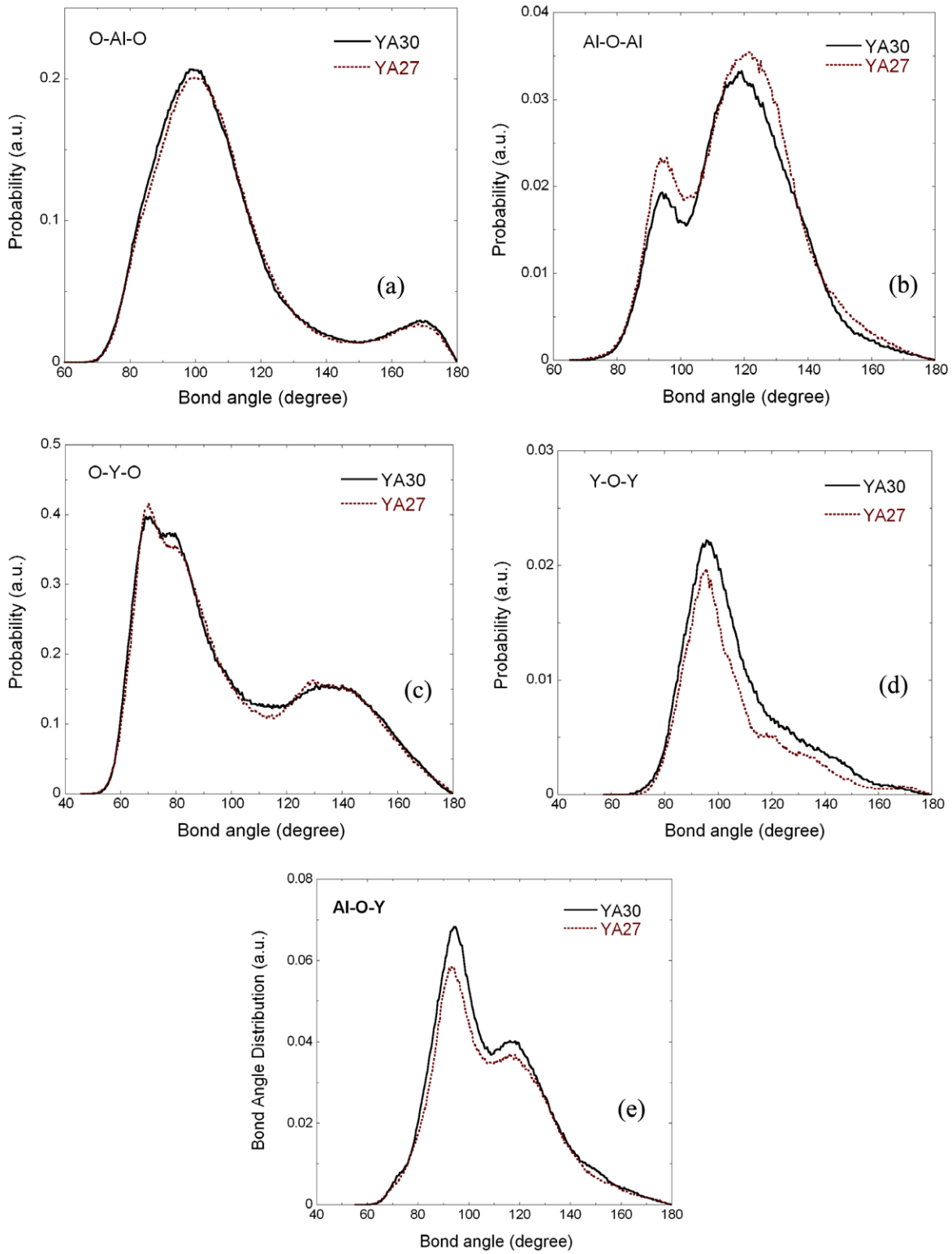

Figure 6. Bond angle distributions for (a) O–Al–O, (b) Al–O–Al, (c) O–Y–O, (d) Y–O–Y and (e) Al–O–Y bonds. (Bond angle distribution calculated with a Al–O cutoff of 2.4 Å and a Y–O cutoff of 3.0 Å.)

exist for the Al–O–Al BADs: a main peak at around 120° and a smaller peak at around 90°. The 90° peak includes contributions from oxygen environment of OAl_2Y_2 and edge-sharing aluminum oxygen polyhedra. The major contribution to the 120° peak is the aluminum oxygen triclusters which give a Al–Al distance of around 3.1 Å which dominates the first peak of Al–Al pair distribution function (figure 5).

The O–Y–O BAD (figure (c)) has two peaks: one major peak at 75° and one small peak at 130°. The Y–O–Y BAD (figure (d)) is dominated by a major peak at around 95°. Like the Al–O–Al BAD, the Al–O–Y BAD (figure 6(e)) shows two

Table 4. Statistics of cation polyhedra connectivity.

	[AlO_x]–[AlO_x]				[AlO_x]–[YO_y]				[YO_y]–[YO_y]			
		Sharing (%)				Sharing (%)				Sharing (%)		
Glass	Total	Corner	Edge	Face	Total	Corner	Edge	Face	Total	Corner	Edge	Face
YA30	1863	87.9	11.9	0.3	2598	67.5	30.4	2.2	692	53.3	38.6	8.0
YA27	2032	87.5	12.3	0.1	2365	70.5	27.9	1.6	512	49.4	38.9	11.7

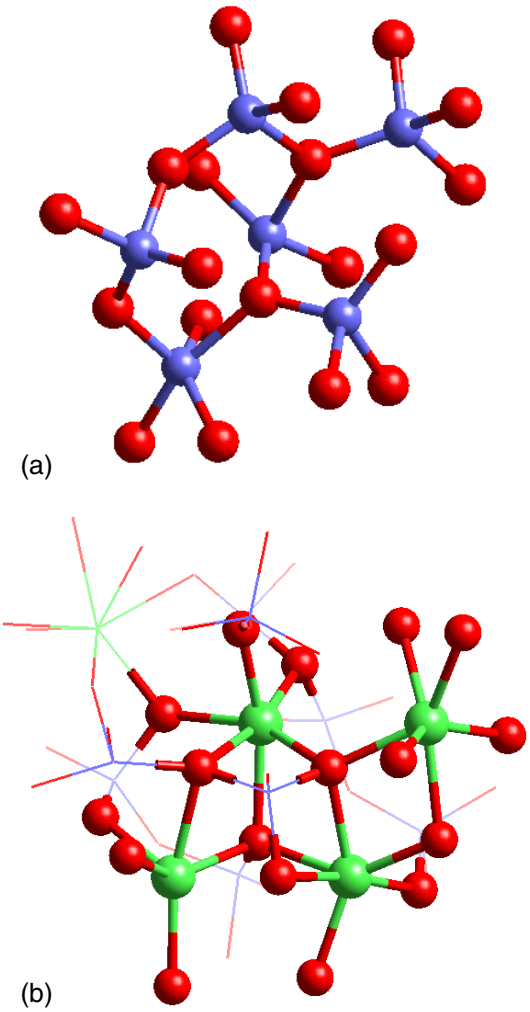

Figure 7. Snapshots of the simulated yttrium aluminate glasses. (a) Region of aluminum–oxygen network with oxygen triclusters, (b) region with edge-sharing yttrium oxygen polyhedra. (Red/dark: oxygen, blue/light: aluminum (small spheres), green/light: yttrium (large spheres)).

peaks: one at 95° and one at 120° but in the Al–O–Y case, the 95° peak is a major one. The 95° peak is mainly due to the corner-sharing aluminum and yttrium oxygen polyhedra.

The aluminum oxide and yttrium oxide polyhedra in the final configuration of the simulated glasses were classified into corner, edge and face sharing. The results of this classification are given in table 4. The most abundant connections are between the [AlO_x] and [YO_y] polyhedra and the least abundant connections are between [YO_y] and [YO_y] polyhedra. Among the [AlO_x]–[AlO_x] connections, the majority (around 87%) are corner sharing and a fraction (around 12%) are edge sharing. Face sharing is below 1%. A considerable amount of edge sharing occurs between [AlO_x]–[YO_y] and [YO_y]–[YO_y] (about 30% and about 40%, respectively). There are also around 10% face sharing in the [YO_y]–[YO_y] connections.

5. Conclusions

The neutron and x-ray structure factors for single phase $(Y_2O_3)_x(Al_2O_3)_{(100-x)}$ glasses, where $x = 27$ and 30, have been calculated using glass structure models obtained from molecular dynamics simulations and compared with experimental measurements. Comparisons of the pair distribution and first order difference functions, bond lengths and coordination numbers between the simulation and experiment have validated the structural models generated by MD simulation, yielding an R-factor of ∼6%. The experimental average Al–O coordination numbers are found to be 4.9 ± 0.2, about 10% larger than 4.4 obtained from the MD simulations. The diffraction data and simulation results for the Y–O coordination numbers agree well, both giving the value of around 6.9. The Al–O polyhedra are dominated by 4-and 5-fold species and the Y–O local coordination are dominated by 6-, 7-and 8-fold polyhedra. An analysis of the oxygen environments reveals a large distribution of combinations. The largest variation found between $x = 27$ and 30 is in the number of aluminum–oxygen triclusters and oxygens surrounded by three Y and a single Al. The most abundant connections are found between the AlO_x and YO_y polyhedra and the majority of AlO_x–AlO_x connections found to be corner shared.

Yttrium aluminates are good glass formers with critical cooling rates ∼50 K s^{-1} and the liquids can be deeply supercooled without crystallizing, although homogeneous single phase glasses can only be formed over a narrow compositional range. The glasses comprise a network of aluminum–oxygen polyhedra and dominated by AlO_4 units. Nonetheless, several rules in the original list of glass former requirements of Zachariasen [32] are not met: namely, an oxygen ion is linked to no more than two glass forming cations and the cation polyhedra are corner shared and not edge or face shared. The Al_3O triclusters present throughout the structure are a major component of the network and are likely to cause the increased viscosity in the deeply supercooled liquids. Yttrium plays a role more closely resembling a modifier although it exhibits substantial connectivity including face-shared species throughout the glass structure. Even though single phase glasses can be formed, the liquids are very fragile with a low viscosity near the equilibrium melting temperature. The many structural configurations present in the

glass are expected to result in a large configurational entropy. The stark differences between the average structure of the glass and the equilibrium crystalline phases in the A–Y binary system further suggests that the glass may form partly due to frustration of the crystallization process.

Acknowledgment

The office of Basic Energy Science, US Department of Energy supported this work under contract number DE-AC02-06CH11357. JD acknowledges support of UNT Research Initiate Grant and startup fund. RTH thanks The Shepherd Chemical Company for use of resources toward this work.

References

[1] Aasland S and McMillan P F 1994 *Nature* **369** 633
[2] Greaves G N, Wilding M C, Fearn S, Langstaff D, Kargl F, Cox S, Van Q V, Majerus O, Benmore C J, Weber R, Martin C M and Hennet L 2008 *Science* **322** 566
[3] Weber J K R, Abadie J G, Hixson A D, Nordine P C and Jerman G A 2000 *J. Am. Ceram. Soc.* **83** 1868
[4] Wilding M C, Benmore C J and McMillanc P F 2002 *J. Non-Cryst. Solids* **297** 143
[5] Tangeman J A, Phillips B L, Nordine P C and Weber J K R 2004 *J. Phys. Chem.* B **108** 10663
[6] Weber R, Benmore C J, Siewenie J, Urquidi J and Key T S 2004 *Phys. Chem. Chem. Phys.* **6** 2048
[7] Johnson B R and Kriven W M 2001 *J. Mater. Res.* **16** 1795
[8] Wilding M C, Wilson M and McMillan P F 2005 *Phil. Trans.* A **363** 589
[9] Nagashio K and Kuribayashi K 2002 *J. Am. Ceram. Soc.* **85** 2353
[10] Skinner L B, Barnes A C, Salmon P S and Crichton W A 2008 *J. Phys.: Condens. Matter* **20** 205103
[11] Cormack A N, Du J and Zeitler T R 2002 *Phys. Chem. Chem. Phys.* **4** 3193
[12] Du J and Cormack A N 2005 *J. Am. Ceram. Soc.* **88** 2978
[13] Du J and Corrales R 2005 *Phys. Rev.* B **72** 092201
[14] Du J and Corrales L R 2006 *J. Non-Cryst. Solids* **352** 3255
[15] Du J 2009 *J. Am. Ceram. Soc.* **92** 1–9
[16] Nose S 1984 *J. Chem. Phys.* **81** 511
[17] Hoover W G 1985 *Phys. Rev.* A **31** 1695
[18] Sears V F 1992 *Neutron News* **3** 26
[19] Hubbell J H, Veigele W J, Briggs E A, Brown R T, Cromer D T and Howerton R J 1975 *J. Phys. Chem. Ref. Data* **4** 471
[20] Cristiglio V, Hennet L, Cuello G J, Johnson M R, Fernandez-Martinez A, Fischer H E, Pozdnyakova I, Zanghi D, Brassamin S, Brun J F and Price D L 2007 *J. Non-Cryst. Solids* **353** 1789
[21] Wilson M and McMillan P F 2004 *Phys. Rev.* B **69** 054206
[22] Wilding M C, McMillan P F and Navrotsky A 2002 *Physica* A **314** 379
[23] Schmucker M and Schneider H 2002 *J. Non-Cryst. Solids* **311** 211
[24] Rütt U, Beno M A, Stempfer J, Jennings G, Kurtz G and Montano P A 2001 *Nucl. Instrum. Methods* A **467** 1026
[25] Urquidi J, Benmore C J, Neuefeind J and Tomberli B 2003 *J. Appl. Crystallogr.* **36** 368
[26] Ellison A J G *et al* 1993 *J. Neutron Res.* **4** 61
[27] Tao J *et al* 2006 *Nucl. Instrum. Methods* A **562** 422
[28] Faber T E and Ziman J M 1965 *Phil. Mag.* **11** 153
[29] Lorch E A 1969 *J. Phys. C: Solid State Phys.* **2** 229
[30] Wilding M C, Benmore C J, Tangeman J A and Sampath S 2004 *Europhys. Lett.* **67** 212
[31] Wright A C 1994 *J. Non-Cryst. Solids* **179** 84
[32] Zachariasen W H 1932 *J. Am. Chem. Soc.* **54** 3841